Design of Nanocrystalline Medium-Voltage Medium-Frequency Three-Phase Transformers for Grid-Connected Applications

Roderick Amir Gomez Jimenez[†], Germán G. Oggier[‡], Roberto A. Fantino [†], Juan Carlos Balda[†] and Yue Zhao[†]

[†] Department of Electrical Engineering, University of Arkansas, Fayetteville Arkansas, USA.
[‡]Grupo de Electrónica Aplicada (GEA)/Instituto de Investigaciones en Tecnologías Energéticas y Materiales Avanzados (IITEMA)
Universidad Nacional de Río Cuarto (UNRC), CONICET, Río Cuarto Córdoba, Argentina.
ragomezj@uark.edu, goggier@ieee.org, rafantin@uark.edu, jbalda@uark.edu and yuezhao@uark.edu

2021 IEEE Energy Conversion Congress and Exposition (ECCE) | 978-1-7281-5135-9/21/$31.00 ©2021 IEEE | DOI: 10.1109/ECCE47101.2021.9595466

***Abstract*—This paper presents the design of a three-phase three-limb high-efficiency medium-voltage medium-frequency transformer with an integrated leakage layer using ribbon-based nanocrystalline cores for three-phase grid-connected applications. The design methodology is based on a custom-core approach developed by a series of design equations that allow the user to select a design that best fits the transformer specifications. A 150-kVA 10-kHz 5-kV-to-400-V three-phase three-limb transformer is designed to validate the proposed design method. In addition, a series of experimental characterisation tests are conducted to measure the performance of the design according do the theoretical performance.**

***Index Terms*—Three-phase dual active bridge (TPDAB), nanocrystalline transformer, medium-frequency transformer (MFT), High voltage transformer, solid-state transformer (SST).**

I. Introduction

Nowadays, the power grid faces the challenge of meeting the new efficiency and flexibility requirements for the future power system of smart-grid technologies. In this challenge, dual active bridge (DAB) is one of the most promising isolated bidirectional DC/DC converters for applications where high efficiency and high-power density are required [1], [2], [3]. Grid connection interface with energy storage [4], grid connection of renewable energy sources [5], and fast charges in automotive [6], are examples of such applications. Furthermore, With the new high voltage fast switching semiconductor devices like SiC and high performance soft-magnetic material, solid-state transformer (SST) exhibits the potential to improve further the power density and efficiency of DC/DC converters and potentially replace the traditional transformers in the power system [7], [8].

The dual-active-bridge converter requires a series inductance with the medium-frequency transformer (MFT) to establish maximum power transfer and shape the current waveform [9]. However, the leakage inductance of a transformer is typically not quite enough for maximum power transfer and controlling its value is challenging. For this reason, MFTs are designed with a reduced leakage inductance, typically a couple of microhenries, which imposes to add an external inductor to meet the required inductance.

Another option consists of adding an extra core into the transformer to meet the power transfer requirements, leading to low losses and a reduced volume design [1], [10]. Three single-phase transformers are typically implemented to obtain a three-phase version since their construction is more straightforward [5], [6]. However, a three-phase three-limb magnetic core exhibiting higher power densities than its single-phase counterpart is now feasible due to customized ribbon-based nanocrystalline cores.

The main contribution of this paper is a high-efficiency three-phase medium-voltage MFT design with high leakage inductance requirements within a single structure for a three-phase DAB converter (TPDAB) used for grid-connected applications. A series of experimental tests will be presented to validate the feasibility of the proposal.

II. Three-Phase Dual Active Bridge DC-DC Converter

The three-phase DAB converter is a well-known topology with the advantages of high-power density and reduced current stresses on the semiconductor devices compared to the single-phase version [11], [12], [13]. In this paper, the converter consists of two three-phase active bridges connected by a three-phase MFT with integrated leakage inductances as shown in Fig. 1.

The primary bridge comprises 10-kV SiC MOSFETs and the secondary of 1.2-kV SiC MOSFETs. As presented in [14], the connections of the three-phase transformer windings modify the converter efficiency and soft-switching range. According to [14], [15], [16], a three-phase transformer for the TPDAB can be designed in a wye-delta (Y - Δ) configuration to yield higher converter efficiency and lower transformer volume. The power transfer of the convert can be determined as follows:

$$P_{rated} = \frac{nV_1V_2}{2\pi f_{sw}L}\phi\left(\frac{2}{3} - \frac{\phi}{2\pi}\right) \quad (1)$$

Authorized licensed use limited to: University of Arkansas. Downloaded on March 01,2022 at 20:00:17 UTC from IEEE Xplore. Restrictions apply.

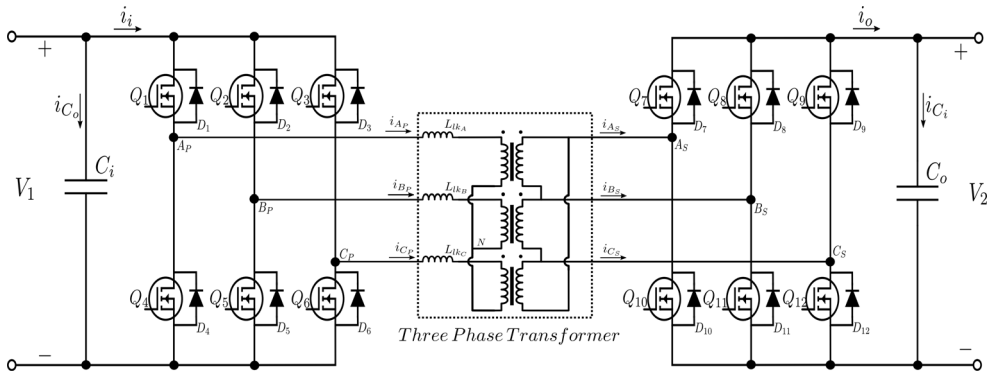

Fig. 1. Three-phase DAB DC/DC converter topology with a wye-delta medium frequency transformer.

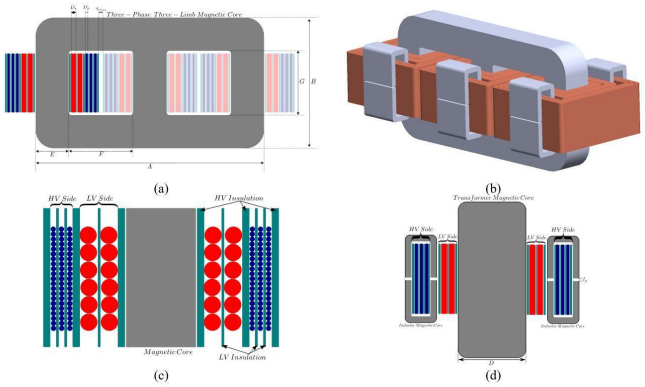

Fig. 2. (a) Three-phase three-limb transformer geometry; (b) Design 3D Model; (c) Winding configuration; (d) Leakage layer configuration.

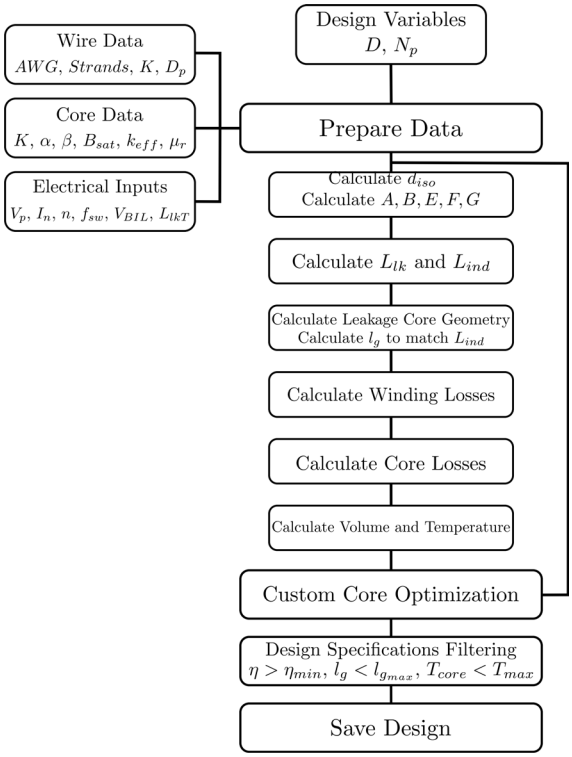

Fig. 3. Custom-Core design methodology flow chart.

where ϕ us the phase-shift, V_1 is the input voltage, V_2 is the output voltage, n is the transformer turn ratio, L is the series inductance or leakage inductance, and f_{sw} is the switching frequency.

III. Three-Phase Three-Limb Transformer Design

Ribbon-based nanocrystalline cores are selected for the transformer. It has been shown in [17], [18] that they exhibit better performance for medium frequencies than soft-magnetic materials like Ferrite and Amorphous. Furthermore, the feasibility of manufacturing ribbon-based cores allows a custom single-core design for three-phase transformers to be implemented with optimal efficiency, volume, and cost, according to previous work presented in [19]. The custom-core design methodology uses the relationship between design specifications and geometrical parameters of the core, so magnetic and copper losses, temperature rise and peak flux density, can be expressed as functions of the core geometry and the number of turns. Fig. 2 (a) shows the proposed three-phase E-type core with geometry dimensions (A, B, F, G, D, E).

The proposed MFT is designed with increased leakage inductance throughout a leakage layer core, as shown in Fig. 2 (b). The leakage inductance referred to the primary side of the transformer using the geometry shown in Fig. 2 (a) can be calculated using (2) and the leakage layer inductance per (3), as presented in [1], [20].

TABLE I
Three-Phase DAB DC/DC Converter Specifications

Parameter	Value	Unit
Rated power	150	kVA
Input voltage	150	kV
Output voltage	400	V
Switching frequency	10	kHz
Series inductances	920	μH

Authorized licensed use limited to: University of Arkansas. Downloaded on March 01,2022 at 20:00:17 UTC from IEEE Xplore. Restrictions apply.

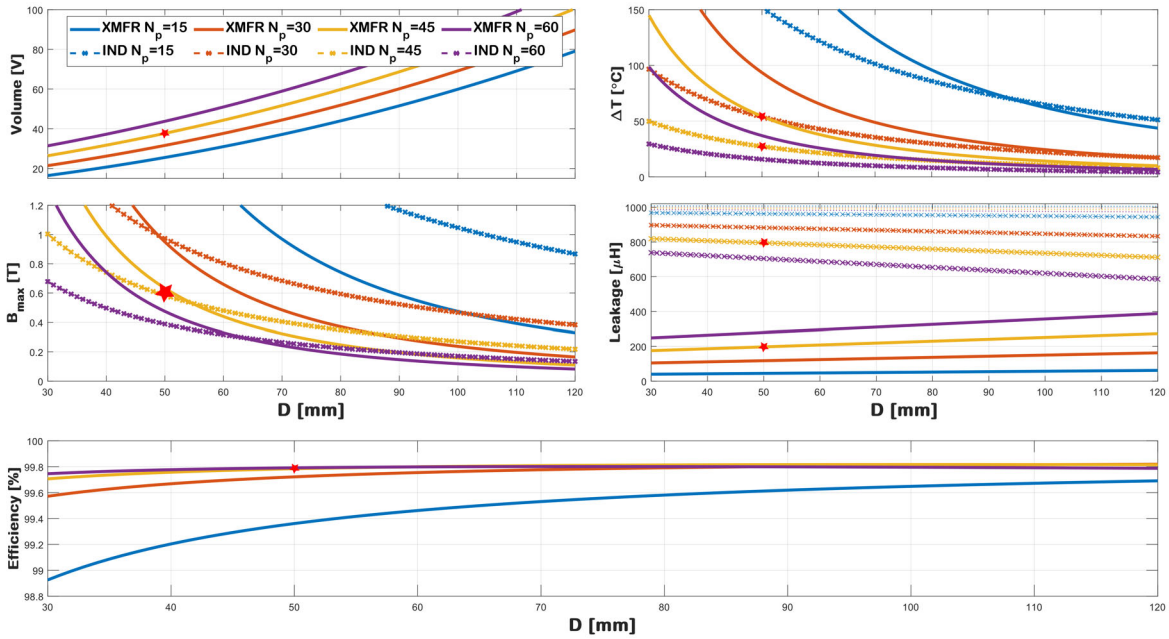

Fig. 4. Three-phase three-limb optimization design results; where XMFR and IND represent the main core and leakage cores parameters, respectively.

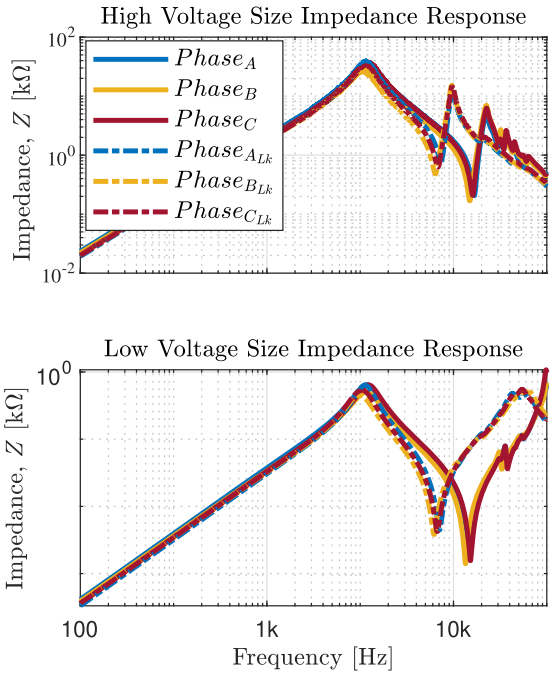

Fig. 5. Open response of primary and secondary side windings over the frequency with and without the external leakage later cores

$$L_{lk} = \frac{\mu_0 \, MLT \, N_p^2}{h} \left[c_1 + \left(\frac{b_1 + b_2}{3} \right) \right] \tag{2}$$

$$L_{int} = \frac{\mu_0 \, A_{c,ind} \, N_p^2}{l_g} \tag{3}$$

where MLT is the mean length turn of the winding, N_p is the number of primary turns, μ_0 is the air permeability, h is the height of the core window, c_1 is the distance between windings, b_1 and b_2 are the copper width of the primary and secondary windings, l_g is the airgap and the $A_{c,ind}$ is the cross-sectional area of the cores used for the leakage layers.

From previous, the total leakage inductance results equal to $L = L_{lk} + 2\,L_{int}$.

The core losses can be estimated using the improved generalized Steinmetz equation (iGSE) (4) [21] which is well accepted and used to design MFTs [19], [20], [22]:

$$P_{v|iGSE} = \frac{1}{T} \int_0^T k_i \left| \frac{dB\,(t)}{dt} \right|^{\alpha} |\Delta B|^{\beta - \alpha} \, dt, \tag{4}$$

where

$$k_i = \frac{k}{(2\pi)^{\alpha-1} \int_0^{2\pi} |cos\,(\theta)|^{\alpha} \, 2^{\beta-\alpha}} \tag{5}$$

The total core losses consist of the losses of the three-limb core plus the losses of the leakage-layer cores. The peak flux density and the core losses on both cores can be calculated as follows:

$$B_{max,\text{XMFR}} = \frac{V_1}{9 f_{sw} N_p A_c} \tag{6}$$

$$B_{max,ind} = I_{max} \frac{\mu_0 N_p}{l_g} \tag{7}$$

$$P_{c|iGSE} = \left(V_{\text{XMFR}} B_{max,\text{XMFR}}^{\beta} + V_{ind} B_{max,ind}^{\beta} \right) \left[k_i f_{sw}^{\alpha} \cdot \right.$$
$$\left. \cdot \; 3^{\alpha-1} \left(2^{\alpha} + 2^{1+\alpha-\beta} \right) \right] \tag{8}$$

Authorized licensed use limited to: University of Arkansas. Downloaded on March 01,2022 at 20:00:17 UTC from IEEE Xplore. Restrictions apply.

where A_c is the cross-sectional area of the three-limb core, V_{XMFR} is the three-limb core volume, V_{ind} is the leakage inductor volume and I_{max} is the peak current of the inductors.

The copper losses can be estimated with

$$P_{cu} = \left(\frac{\delta \rho_{cu} N_p}{A_{litz}}\right)\left[MLT_p/S_p I_{p\,RMS}^2 + MLT_s/S_s I_{s\,RMS}^2\right] \tag{9}$$

where S_p, S_s and A_{litz} are Litz wire specifications parameters; MLT_p and MLT_s are the mean length per turns and δ is a factor to consider the increase on copper losses due to the ac resistance. The temperature rise on the core can be approximated using $\Delta T = 450\,(P_{core}/A_{surf})^{0.826}$; presented in [20].

Using these equations as a function of the core thickness D and the primary number of turns N_p, the optimization algorithm presented in Fig. 3 can be implemented to select an optimal design for the TPDAB. This algorithm aims to find the core thickness and the number of turns that better fit the design specifications within operational boundaries (volume, losses, and temperature). Fig. 4 illustrates the design results of the optimization algorithm and Table II shows the selected prototype for the TPDAB.

IV. Three-Phase Three-Limb Transformer Characterization

A. Impedance Response Analysis

The transformer impedance is measured using the Omicron Bode 100 a Vector Network Analyzer. The open response of the impedance for the high voltage side and low voltage side are illustrated in Fig. 5. The integration of the leakage cores into the primary winding produces few changes in the total impedance of the transformer. However, the resonance point due to the intra-winding and inter-winding parasitic capacitances is shifted to lower frequencies and it slightly dampens the resonance. This response is observed for either primary or secondary windings. On the other hand, Fig. 6 shows the leakage inductance from the primary side winding for each phase. The integration of the two leakage cores to the side of the primary winding perpendicular to the main core increased the leakage inductance per phase from 246 μH to about 960 μH; leakage required for power transfer of the TPDAB. Table IV states the impedance at switching frequency for each of the phases.

TABLE II
Three-Phase Three-Limb Transformer Design Results

Parameter	Value	Unit
P_{core}	210	W
P_{ind}	115	W
P_{cu}	225	W
η	99.63	%
ΔT_{XMFR}	46	°C
ΔT_{IND}	28	°C
Volume	20	L
L_{lkT}	942	μH

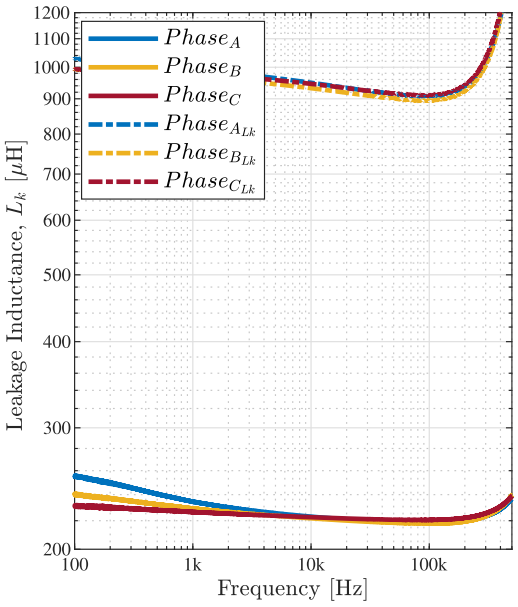

Fig. 6. Leakage impedance response of primary winding with and without the external leakage layer cores

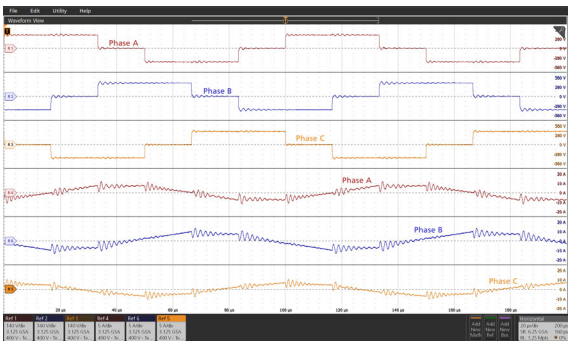

Fig. 7. Open-Circuit test results at 400 V on the delta side of the transformer

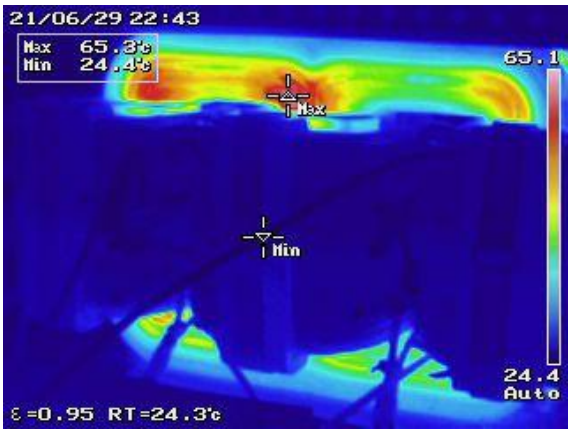

Fig. 8. Thermal response of the transformer under open-circuit at nominal voltage

Authorized licensed use limited to: University of Arkansas. Downloaded on March 01,2022 at 20:00:17 UTC from IEEE Xplore. Restrictions apply.

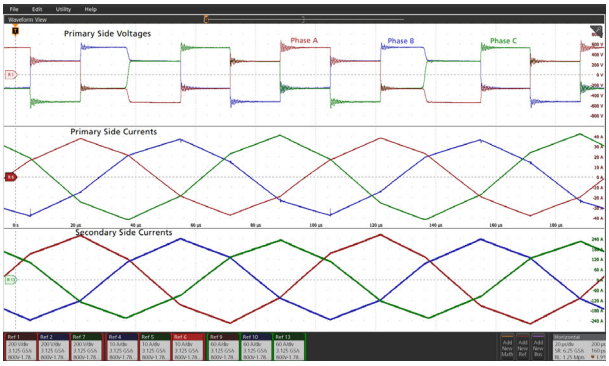

Fig. 9. Short-circuit test of the three-phase $Y - \Delta$ transformer at nominal operating current

B. Core Loss Characterization

The characterization of the core losses of the transformer was divided into two sections. First, the transformer core losses without the leakage cores are measured to account for the extra losses when those cores are integrated to the design. Then, a test to measured the core losses with the additional cores can be performed. The open-circuit test is then performed from the low-voltage side. Fig. 7 shows the results of the core-loss with the integrated leakage core, taken with the Tektronix MSO8 Oscilloscope. The open-circuit test showed that the core loss of the three-limb core is about 500 W, which is 25% more than the losses without the extra cores 400 W. From the open circuit test, it can be seen that the parasitic capacitance for a tree-phase transformer at high voltage becomes a critical point for further design optimization. The parasitic capacitance of windings leads to a resonance of 1.66 MHz on each phase. This frequency decreases to 680 kHz when the extra core are used. The designed winding was tested on a single-winding configuration and showed a resonance frequency of 6.8 MHz and 6.32 MHz with and without the extra cores. A thermal image of the core under nominal core losses is shown in Fig. 8, showing a temperature rise of about $41°C$.

C. Copper Loss Characterization

The copper loss due to the primary and secondary windings can be measured by performing a short-circuit test (SC) at nominal current. Fig. 9 displays the experimental results of the SC test at $I_{SC} \approx 23.75\ A_{RMS}$ for a three-phase Wye-Delta winding. The copper loss per phase was $P_{cu,\phi} \approx 90\,W$ which resulted in $270\,W$ total loss due to the resistance of the windings.

TABLE III
THREE-PHASE THREE-LIMB TRANSFORMER COPPER LOSS CHARACTERIZATION

Parameter	Theoretical	Impedance Analyzer	Single-Phase Test	Three-Phase Test
$P_{cu,\phi}$	75 W	93.5 W	91 W	90 W
$P_{cu,tot}$	225 W	280.5 W	273 W	270 W

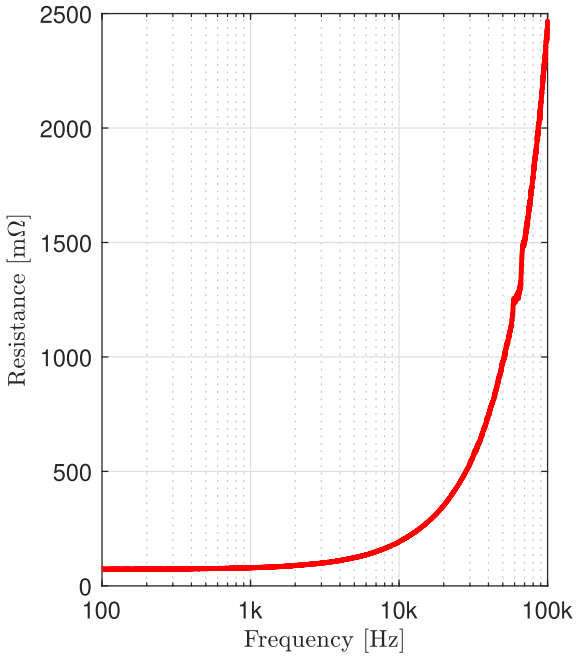

Fig. 10. Per-phase short-circuit resistance seem from the high voltage side

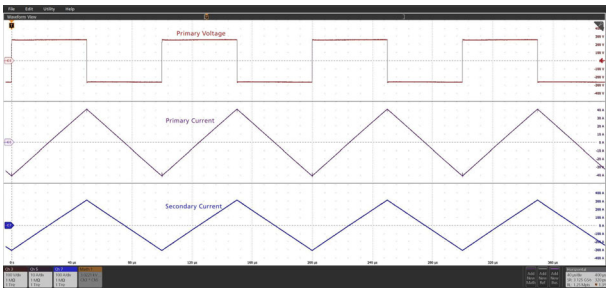

Fig. 11. Single-phase equivalent short-circuit test at nominal rms current

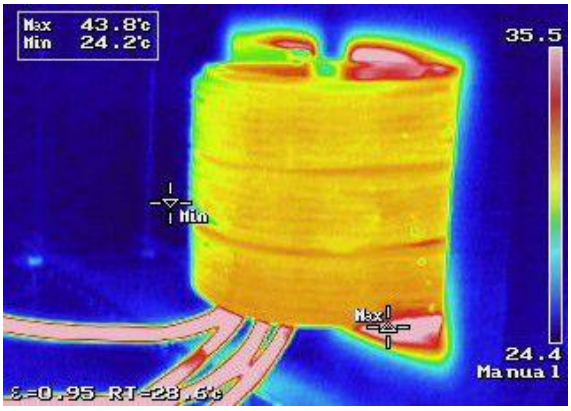

Fig. 12. Thermal response of the transformer winding under nominal current

This experimental result can be further validated by using the series resistance of the primary winding while the

Authorized licensed use limited to: University of Arkansas. Downloaded on March 01,2022 at 20:00:17 UTC from IEEE Xplore. Restrictions apply.

TABLE IV
THREE-PHASE THREE-LIMB TRANSFORMER IMPEDANCE CHARACTERIZATION

Phase	L_m w/o extra cores	L_m w/ extra cores	L_{lk} w/o extra cores	L_{lk} w/ extra cores
A	29.902 mH	28.095 mH	237 μH	948 μH
B	29.983 mH	28.028 mH	236 μH	949 μH
C	29.862 mH	28.113 mH	235 μH	946 μH

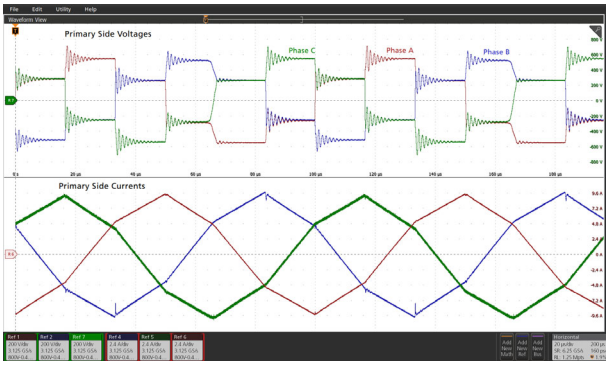

Fig. 13. Short-circuit test on the wye side of the transformer with leakage cores

Fig. 14. Three-phase three-limb transformer

secondary is short-circuited. The frequency response of this resistance is shown in Fig. 10. The total per-phase winding resistance is $R_{SC,\phi} \approx 165.82\, m\Omega$ which at nominal current ($I_{SC} \approx 23.75\, A_{RMS}$) results in a loss of $P_{cu,\phi} \approx 93.5\, W$. In addition, a single-phase short-circuit test shown in Fig. 11 resulted in a copper loss of $P_{cu,\phi} \approx 91\, W$. Finally, a thermal image of the winding under nominal current is displayed in Fig. 12. Table III summarized the experimental results of the copper loss measurements. While the experimental measurements are consistent, the theoretical model slightly underestimates the ac copper losses and does not account for the added resistance of the winding terminals and connections.

D. Leakage Inductance Characterization

The leakage impedance of each phase can be obtained using the vector network analyzer as shown in section A; nevertheless, the leakage inductance can be obtained from the short-circuit test. The slope of the short-circuit current in Fig. 9 corresponds to a per winding leakage impedance of $L_{lk} \approx 236\, \mu H$ for phase B. The added magnetic cores increased the leakage inductance to the required value to achieve maximum power transfer at nominal voltage and current. A low current short-circuit test with the extra leakage cores is illustrated in Fig. 13. The current slope corresponds to a per winding leakage impedance of $L_{lk} \approx 965\, \mu H$ which satisfies the leakage requirements. Refer to Table IV for a comparison of the impedance with and without the extra cores.

ACKNOWLEDGMENT

The authors are grateful for the financial support from the National Science Foundation Industry/University Cooperative Research Center on Grid-connected Advanced Power Electronics Systems (GRAPES).

V. CONCLUSION

A custom-core medium-frequency transformer design methodology was presented and experimentally validated for a 150-kVA 10-kHz three-phase three-limb transformer shown in Fig. 14 for a three-phase high-voltage to low-voltage dual active bridge. The open-circuit test characterization at nominal voltage resulted in a core loss of about 500 W while the short-circuited test showed a total loss of about 280 W. The characterization of the transformer yield a high efficiency of 99.48 % operating at nominal conditions. Furthermore, the impedance characterization of the transformer showed that with the addition of the extra layer of core, the transformer could meet the leakage inductance requirements for power transfer without the need for a complex winding structure. On the other hand, the impedance characterization raised the issue of the parasitic capacitances of high voltage windings. As illustrated in Fig. 7, these inter-winding and intra-winding parasitic capacitances cause medium-frequency resonances on the current. Compare to the single-phase winding arrangement, a three-phase transformer presents 4 times lower frequency resonances. Future work includes a more comprehensive experimental characterization of the transformer with the added leakage core working within the three-phase converter. In addition, further work on the diminishment of the parasitic capacitance will be conducted to mitigate the resonance seen on the transformer current.

REFERENCES

[1] B. Cougo and J. W. Kolar, "Integration of Leakage Inductance in Tape Wound Core Transformers for Dual Active Bridge Converters," *7th International Conference on Integrated Power Electronics Systems (CIPS)*, 2012, pp. 1-6.

[2] S. Inoue and H. Akagi, "A Bidirectional Isolated DC–DC Converter as a Core Circuit of the Next-Generation Medium-Voltage Power Conversion System," *in IEEE Transactions on Power Electronics*, vol. 22, no. 2, pp. 535-542, March 2007.

Authorized licensed use limited to: University of Arkansas. Downloaded on March 01,2022 at 20:00:17 UTC from IEEE Xplore. Restrictions apply.

[3] R. W. A. A. De Doncker, D. M. Divan and M. H. Kheraluwala, "A three-phase soft-switched high-power-density DC/DC converter for high-power applications," *in IEEE Transactions on Industry Applications*, vol. 27, no. 1, pp. 63-73, Jan.-Feb. 1991.

[4] H. Zhou and A. M. Khambadkone, "Hybrid Modulation for Dual-Active-Bridge Bidirectional Converter With Extended Power Range for Ultracapacitor Application," *in IEEE Transactions on Industry Applications*, vol. 45, no. 4, pp. 1434-1442, July-aug. 2009.

[5] M. Kaymak, R. W. De Doncker and T. Jimichi, "Design and Verification of a Medium-Frequency Transformer in a Three-Phase Dual-Active Bridge DC-DC Converter for Medium-Voltage Grid Connection of Offshore Wind Farms," *IEEE Applied Power Electronics Conference and Exposition (APEC)*, 2020, pp. 2694-2701.

[6] S. Haghbin, M. Alatalo, F. Yazdani, T. Thiringer and R. Karlsson, "The Design and Construction of Transformers for a 50 kW Three-Phase Dual Active Bridge DC/DC Converter," *IEEE Vehicle Power and Propulsion Conference (VPPC)*, 2017, pp. 1-5.

[7] G. Ortiz, M. Leibl, J. W. Kolar and O. Apeldoorn, "Medium frequency transformers for solid-state-transformer applications — Design and experimental verification," *IEEE 10th International Conference on Power Electronics and Drive Systems (PEDS)*, 2013, pp. 1285-1290.

[8] C. Leung, S. Dutta, S. Baek and S. Bhattacharya, "Design considerations of high voltage and high frequency three phase transformer for Solid State Transformer application," *IEEE Energy Conversion Congress and Exposition*, 2010, pp. 1551-1558.

[9] G. Ortiz, J. Biela, D. Bortis and J. W. Kolar, "1 Megawatt, 20 kHz, isolated, bidirectional 12kV to 1.2kV DC-DC converter for renewable energy applications", *The International Power Electronics Conference - ECCE ASIA -*, 2010, pp. 3212-3219.

[10] M. Pavlovsky, S. W. H. de Haan and J. A. Ferreira, "Winding losses in high-current, high-frequency transformer foil windings with leakage layer," *37th IEEE Power Electronics Specialists Conference*, 2006, pp. 1-7.

[11] D. Segaran, D. G. Holmes and B. P. McGrath, "Comparative analysis of single and three-phase dual active bridge bidirectional DC-DC converters," *Australasian Universities Power Engineering Conference*, 2008, pp. 1-6.

[12] H. van Hoek, M. Neubert, A. Kroeber and R. W. De Doncker, "Comparison of a single-phase and a three-phase dual active bridge with low-voltage, high-current output," *International Conference on Renewable Energy Research and Applications (ICRERA)*, 2012, pp. 1-6.

[13] A. K. Tripathi, K. Hatua and S. Bhattacharya, "A comparative study of three-phase dual active bridge topologies and their suitability for D-Q mode control," *IEEE Energy Conversion Congress and Exposition (ECCE)*, 2012, pp. 1719-1724.

[14] R. O. Núñez, G. G. Oggier, F. Botterón, and G. O. García, "A comparative study of Three–Phase Dual Active Bridge Converters for renewable energy applications," *Sustainable Energy Technologies and Assessments - Elsevier*, vol. 23, pp. 1–10, Oct. 2017.

[15] K. Jin and C. Liu, "A Novel PWM High Voltage Conversion Ratio Bidirectional Three-Phase DC/DC Converter With Y–Δ Connected Transformer," *IEEE Trans. Power Electron.*, vol. 31, no. 1, pp. 81-88, Jan. 2016.

[16] N. H. Baars, J. Everts, C. G. E. Wijnands and E. A. Lomonov, "Performance Evaluation of a Three-Phase Dual Active Bridge DC–DC Converter With Different Transformer Winding Configurations," *IEEE Trans. Power Electron.*, vol. 31, no. 10, pp. 6814-6823, Oct. 2016.

[17] M. S. Rylko, K. J. Hartnett, J. G. Hayes and M. G. Egan, "Magnetic Material Selection for High Power High Frequency Inductors in DC-DC Converters," *Twenty-Fourth Annual IEEE Applied Power Electronics Conference and Exposition*, 2009, pp. 2043-2049.

[18] W. Shen, F. Wang, D. Boroyevich and C. W. Tipton IV, "High-Density Nanocrystalline Core Transformer for High-Power High-Frequency Resonant Converter," *IEEE Trans. Ind. App.*, vol. 44, no. 1, pp. 213-222, Jan.-feb. 2008.

[19] S. Christian, R. A. Fantino, R. Amir Gomez, J. C. Balda, Y. Zhao and G. Zhu, "150-kW Three-Port Custom-Core Transformer Design Methodology," *IEEE Applied Power Electronics Conference and Exposition (APEC)*, 2020, pp. 1020-1024.

[20] W. T. Mclyman, *Transformer and Inductor Design Handbook - Third Edition, Revised and Expanded,* 2004.

[21] K. Venkatachalam, C. R. Sullivan, T. Abdallah and H. Tacca, "Accurate prediction of ferrite core loss with nonsinusoidal waveforms using only Steinmetz parameters," *IEEE Workshop on Computers in Power Electronics Proceedings*, 2002, pp. 36-41.

[22] M. Mogorovic and D. Dujic, "100 kW, 10 kHz Medium-Frequency Transformer Design Optimization and Experimental Verification," *in IEEE Transactions on Power Electronics*, vol. 34, no. 2, pp. 1696-1708, Feb. 2019.

Authorized licensed use limited to: University of Arkansas. Downloaded on March 01,2022 at 20:00:17 UTC from IEEE Xplore. Restrictions apply.